Int. J. Simul. Multidisci. Des. Optim. **3**, 297-306 (2009)

DOI: 10.1051/ijsmdo:2009002

Available online at:
http://www.ijsmdo.org

Topology optimization of multiphase-material structures under design-dependent pressure loads

Tong Gao[1], Wei-hong Zhang[1a]
[1] Engineering Simulation and Aerospace Computing (ESAC), Northwestern Polytechnical University, 710072, Xi'an, Shaanxi, China

Received 26 June 2008, Accepted 02 November 2008

Abstract – In this paper, design-dependent pressure loads are addressed for topology optimization problems of multiphase material structures. The modeling of unidirectional load distribution with respect to the material density is studied and mathematical formulations of exponential form are established for the first time to model unidirectional pressure loads on the moving surface and contact surface of fixed shape, respectively. In both load cases, sensitivity analysis scheme of the structural compliance is developed to show the effects of the design–dependent loads. By means of 2D and 3D numerical examples, comparative studies are performed in detail to show the effects of different load cases upon the optimal configurations. It is seen that the proposed design procedure is reliable to deal with the design-dependent load cases.

Key words: Topology optimization, design-dependent pressure loads, load distribution, sensitivity analysis

1 Introduction

Here starts the main part of the paper. You can finish your paper first and then copy all your texts, figures and tables into this template. And the "Format brush" in MS-Word may be helpful.

This paragraph shows how to use some references. Within this scope, optimal support locations were found by Rozvany [1], Mroz and Rozvany [2], Prager and Rozvany [3], Szelag and Mroz [4] to improve elastic and plastic responses of beams. Likewise, Rozvany and Mroz [5], Olhoff and Taylor [6], Olhoff and Akesson [7] discussed the column support optimization for buckling load maximization.

In recent years, various optimization models and methods have been presented to address the structural design problems. Among others, topology optimization is an advanced research topic. It could be considered as a 0-1 discrete problem. The basic approach is to transform the discrete problem into a continuous one, such as the homogenization method (Bendsøe and Kikuchi [5]), the SIMP (Solid Isotropic Material with Penalization) method (Bendsøe [3], Bendsøe and Sigmund [6]) and the RAMP (Rational Approximation of Material Properties) method (Stolpe and Svanberg [20]). Nevertheless, the considered problems are mostly limited to fixed load conditions. Namely, whatever the variation of the structural configuration is, the applied loads remain unchanged. In practice, many structures need to be designed for optimal configurations under such a type of load that changes with respect to the material layout, i.e., the so-called design-dependent load (Chen and Kikuchi, [8]).

By definition, the design-dependent loads are those whose values, locations or directions depend upon the structure itself. Here, it is necessary to highlight two points. Firstly, as the loads vary during the design iteration process, a proper load model is needed for their updating in terms of design variables. Secondly, when the objective function to be minimized is still defined as the structural compliance, the sensitivity of the latter will change its sign instantly during the optimization iteration due to the effect of the design-dependent loads so that the objective function is no longer a decreasing monotonic function. This implies that more material might make the structure less rigid. Instead, the sensitivity is always negative under fixed load conditions, i.e., more materials, more rigid the structure. To clarify the discussion, considered design-dependent loads are classified in the following presentation.

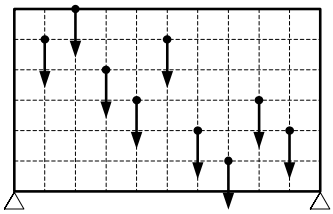

(a) Model and boundary condition

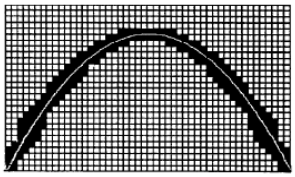

(b) Optimal result of Fuchs and Moses [12]

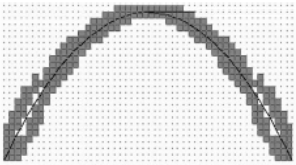

(c) Optimal result of Yang et al. [24]

Fig. 1 Optimal results related to transmissible loads

"Transmissible" or "sliding" loads: To the authors' knowledge, "transmissible" or "sliding" loads might be the design-dependent loads that were firstly investigated in the work of Rozvany and Prager [17]. According to Fuchs and Moses [12], a transmissible force is a force of given magni-

[a] Corresponding author: zhangwh@nwpu.edu.cn

Article available at http://www.ijsmdo.org or http://dx.doi.org/10.1051/ijsmdo/2009002

tude and direction which can be applied at any point along the action line of the force. As illustrated in Fig. 1(a), each force attached to the universe structure is movable vertically. Fuchs and Moses [12] studied the topology optimization of structures under transmissible loads and the so-called "Prager structure" is obtained. Likewise, Yang et al. [24] solved this problem with ESO/BESO (Evolutionary Structural Optimization and Bi-direction Evolutionary Structural Optimization) method. As shown in Fig. 1, similar optimal results are obtained with the height-to-length ratio being 0.479 and 0.48, respectively whereas the analytical solution obtained by Rozvany and Prager [17] has a height-to-length ratio of 0.43.

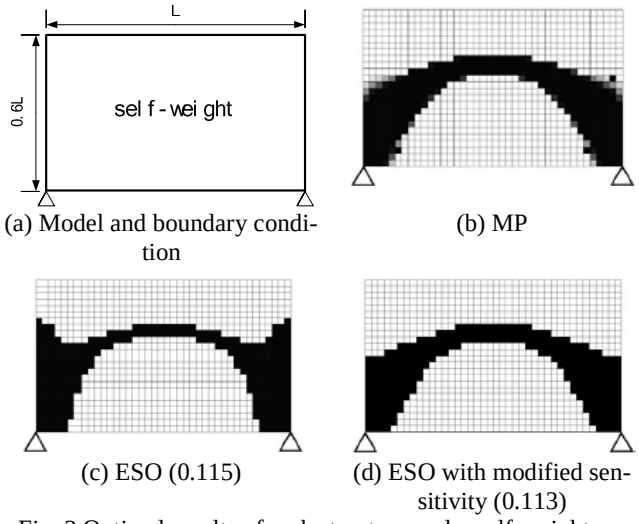

(a) Model and boundary condition (b) MP

(c) ESO (0.115) (d) ESO with modified sensitivity (0.113)

Fig. 2 Optimal results of arch structure under self-weight load (Ansola et al. [2])

Body force: This includes inertial load (e.g., structural self-weight, translational inertial load and centrifugal load) and heat generation rate of the thermal problem. In structural topology optimization, the location and direction of body force usually keep fixed whereas the magnitude will vary with the addition and deletion of materials in the optimization process. In other words, no material, no load. Bruyneel and Duysinx [7] investigated the topology optimization of structures under self-weight loading with SIMP and different MMA (Method of Moving Asymptotes) approximation schemes. Yang et al. [24] applied the ESO/BESO method to solve the same problem. In the work of Ansola et al. [2], obtained solutions are found to be not exactly the same. As shown in Fig. 2, under the self-weight loading, the MP method produces an arch-like structure, whereas the ESO method gives rise to a more compliant solution for which two columns are generated at both sides on the top of supports and joined together with a slender arch. For this reason, Ansola et al. [2] introduced the volume constraint to modify the sensitivity formula, so that the improved result agrees well with that obtained by the MP method as observed in Fig. 2(d). Besides, combined centrifugal and external loads were addressed by Turteltaub and Washabaugh [23] to show the influence of relative magnitude of both loads on the optimal design of the rotating prismatic structure. The heat generation rate was investigated by Gao et al. [14] for topology optimization of the steady heat conduction problem with the BESO method. It is necessary to notice that the material removal will reduce the body force and in the limit case the design problem will become singular when the structure is only solicited by the body force.

Surface contact pressure load: The pressure load is characterized by the applied surface, load magnitude and load direction. Here, two cases of surface pressure loads are considered:

Case 1: Unidirectional pressure load on contact surface of fixed shape. This type of load is applied on a loading surface of specific shape. The surface contact area may change and the load will be redistributed in the design process while the amount of total load remains constant and the loading direction is unchanged during the topology optimization. The typical example is the design of a load support structure pressured by a rigid object.

Case 2: Unidirectional pressure load on moving surface: The difference between this type of load and the preceding one lies in that the pressure load follows the variation of the loading surface being designed during the structural optimization while the load magnitude and the direction remain unchanged. The typical example is the snow weight pressure acting on a civil structure. Note that the hydrostatic pressure load is similar but the loading direction is always normal to the loading surface.

Until now , existing work has been mainly focused on the hydrostatic pressure load and the unidirectional pressure load on moving surface. Few works are found on the pressure load of Case 1. Bendsøe [4] studied the simultaneous optimization of the structure topology and shape under the hydrostatic pressure load and the structure was re-meshed after each iteration. The same problem was addressed by Hammer and Olhoff [15], Du and Olhoff [9-10] who used the fixed grid to avoid the re-meshing. In addition, the loading position was modeled in each iteration as a smooth surface that is determined by the local interpolation of the material densities and then loaded by the pressure. Fuchs and Shemesh [13] defined the loading surface independent of element density distribution and used very low Young's modulus to model the water as highly compliant material. Chen and Kikuchi [8] solved the hydrostatic pressure problem with a special strategy by which the design domain was transformed to three-phase materials (solid, void and hydrostatic fluid) and the hydrostatic pressure along the solid-fluid interface was simulated as the thermal expansion effect of both phases of different thermal expansion coefficients. Later, the level set method was applied to determine the moving boundary of pressure load (Allaire et al. [1], Liu et al. [16]). Recently, Sigmund and Clausen [19] suggest a mixed displacement-pressure finite element formulation by which the pressure loading surface doesn't need to parameterize for the hydrostatic pressure problem. However, as this method is based on the special finite element formulation, it is difficult to implement it in the common engineering finite element software. The unidirectional pressure load on moving surface is sometimes treated as a special case of hydrostatic pressure, typically in the works of Du and Olhoff [9], Chen and Kikuchi [8]. Alternatively, The ESO method was applied by Yang et al. [24] to solve this problem.

In Fig. 3, optimal results obtained by Du and Olhoff [9] are compared for fixed pressure load, hydrostatic pressure

and unidirectional pressure load. Obviously, the variations of load locations and directions lead to different optimal designs. Under hydrostatic pressure and unidirectional pressure loads, the solutions are arch-like structures, while some vertical columns supporting the non-designable loading top deck are obtained in the case of fixed load. Therefore, how the pressure load is properly modeled is a key issue dominating the optimal configuration. This is the motivation of the current work.

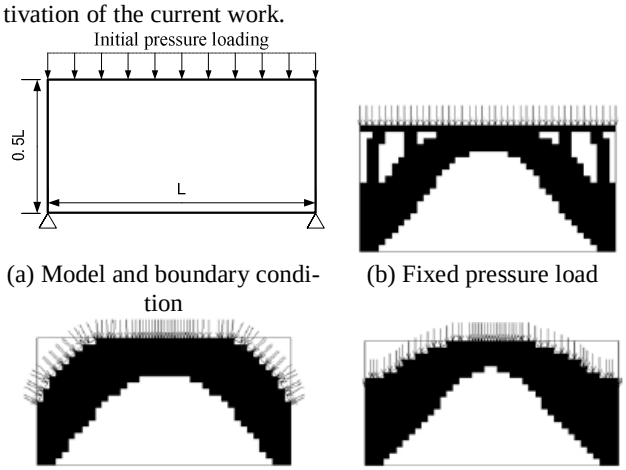

(a) Model and boundary condition (b) Fixed pressure load

(c) Hydrostatic pressure load (d) Unidirectional pressure load

Fig. 3 Optimal results under different pressure loads (Du and Olhoff [9])

In this paper, the main work is focused on the structural topology optimization subjected to unidirectional pressure loads. The maximum stiffness design is sought for structures consisting of multiphase materials.

Firstly, we present the mathematical formulation of the maximum stiffness problem with multiphase materials. Secondly, the load distribution model is established explicitly in terms of density variables for each type of pressure load. Discussions are made about the design-dependent effects of both types of pressure loads in sensitivity analysis of the structural compliance. It is shown that the explicit form of the pressure load can favor the analytical sensitivity analysis efficiently. Finally, some 2D and 3D representative examples are solved with the help of the developed force model and design procedure. Solutions associated with two load cases are investigated and compared with existing solutions to show the validity of the proposed models and methods. Furthermore, the influence of the parameters, such as the material volume fraction, the size of designable and non-designable domains upon the optimal configurations are presented and analyzed.

2 Topology optimization of structures with multiphase materials

Basically, the purpose of structural topology optimization is to find such a topological configuration that has the maximum overall mean stiffness or minimum compliance for the prescribed material cost. The design variables are often defined by the element pseudo-densities and the SIMP model is often used both to penalize the element stiffness and to convert the discrete problem into a continuous one.

Consider a structure consisting of one solid isotropic material of Young's modulus E(1), the SIMP interpolation model corresponds to

$$E\left(x_i\right) = x_i^r E^{(1)} \tag{1}$$

where x_i is the pseudo-density design variable of element i, that represents the absence (0) or presence (1) of the material. r is the penalization factor. The void area can be therefore considered as a material whose Young's modulus is zero. Generally, when the structure consists of multiphase materials, the SIMP model can be written in the following way.

2.1 Two-phase materials

In this case, the SIMP interpolation model corresponds to

$$\begin{aligned} &E\left(\mathbf{x}_i\right) = x_{i1}^r E^{(1)} + (1 - x_{i1}^r) E^{(0)} \\ &\mathbf{x}_i = \left\{x_{ij}\right\} \quad \left(i = 1, \ldots, n; \quad j = 1\right) \\ &E^{(1)} > E^{(0)} \end{aligned} \tag{2}$$

where x_{i1} is the design variable of element i and n refers to the element number. $E^{(1)}$ and $E^{(0)}$ are the Young's moduli of two materials, respectively. Herein, the structure is composed of one solid material and void if $E^{(0)}$=0. Consequently, the structural topology optimization problem can be written as

$$\begin{aligned} &\text{find:} \quad \left\{x_{i1}\right\} \quad \left(i = 1, \ldots, n\right) \\ &\text{minimize: } C = \mathbf{u}^{\mathrm{T}} \mathbf{K} \mathbf{u} \\ &\text{subject to: } \mathbf{F} = \mathbf{K} \mathbf{u} \\ &\sum_{i=1}^{n} V_i x_{i1} \le vf_1 \cdot \sum_{i=1}^{n} V_i \end{aligned} \tag{3}$$

where vf_1 is the prescribed volume fraction of material 1. V_i denotes the volume of element i. Usually, a lower bound, $x_{\min}$, e.g., 10^{-3}, is introduced for x_{i1} to avoid the singularity of the element stiffness matrix during the design iteration.

Based on the finite element system equation, the differentiation results in

$$\frac{\partial \mathbf{K}}{\partial x_{ij}} \mathbf{u} + \mathbf{K} \frac{\partial \mathbf{u}}{\partial x_{ij}} = \frac{\partial \mathbf{F}}{\partial x_{ij}} \tag{4}$$

so that

$$\frac{\partial \mathbf{u}}{\partial x_{ij}} = \mathbf{K}^{-1} \frac{\partial \mathbf{F}}{\partial x_{ij}} - \mathbf{K}^{-1} \frac{\partial \mathbf{K}}{\partial x_{ij}} \mathbf{u} \tag{5}$$

The sensitivity of the mean compliance can thus be expressed as

$$\frac{\partial C}{\partial x_{ij}} = \frac{\partial}{\partial x_{ij}} (\mathbf{F}^{\mathrm{T}} \mathbf{u}) = \frac{\partial \mathbf{F}^{\mathrm{T}}}{\partial x_{ij}} \mathbf{u} + \mathbf{F}^{\mathrm{T}} \frac{\partial \mathbf{u}}{\partial x_{ij}} \tag{6}$$

The substitution of eq. (4) into eq. (6) yields

$$\frac{\partial C}{\partial x_{ij}} = 2 \frac{\partial \mathbf{F}}{\partial x_{ij}} \mathbf{u}^{\mathrm{T}} - \mathbf{u}^{\mathrm{T}} \frac{\partial \mathbf{K}}{\partial x_{ij}} \mathbf{u} \tag{7}$$

In the right hand, the first term represents the effect of design-dependent load. The evaluation of $\partial \mathbf{F} / \partial x_{ij}$ depends on how the force is modeled in terms of x_{ij}. This is the key

issue of the current work. For two-phase materials, the second term can be evaluated based on the SIMP model of eq. (2)

$$\frac{\partial \mathbf{K}}{\partial x_{i1}} = \frac{\partial \mathbf{K}_i}{\partial x_{i1}} = r x_{i1}^{r-1}\left(\mathbf{K}^{(1)} - \mathbf{K}^{(0)}\right) \tag{8}$$

$\mathbf{K}^{(1)}$ and $\mathbf{K}^{(0)}$ refer to the element stiffness matrices related to $E^{(1)}$ and $E^{(0)}$, respectively. Thus, the substitution of $\partial\mathbf{F}/\partial x_{i1}$ and $\partial\mathbf{K}/\partial x_{i1}$ to eq. (7) yields the sensitivity of the objective function.

If the concerned load is fixed and not design-dependent, eq. (7) can be simplified as

$$\frac{\partial C}{\partial x_{ij}} = -\mathbf{u}^{\mathrm{T}} \frac{\partial \mathbf{K}}{\partial x_{ij}} \mathbf{u} \tag{9}$$

The substitution of eq. (8) into eq. (9) then gives rise to the sensitivity of the structure compliance for two-phase material.

$$\begin{aligned}\frac{\partial C}{\partial x_{i1}} &= -r x_{i1}^{r-1} \mathbf{u}_i^{\mathrm{T}}\left(\mathbf{K}_i^{(1)} - \mathbf{K}_i^{(0)}\right)\mathbf{u}_i \\ &= -r x_{i1}^{r-1}(E^{(1)} - E^{(0)})\mathbf{u}_i^{\mathrm{T}}\overline{\mathbf{K}}_i\mathbf{u}_i\end{aligned} \tag{10}$$

It has the constant sign for $0 \le x_{i1} \le 1$. Note that $\mathbf{K}_i^{(1)} = E^{(1)}\overline{\mathbf{K}}_i$, $\mathbf{K}_i^{(0)} = E^{(0)}\overline{\mathbf{K}}_i$.

2.2 Three-phase materials

The two-phase SIMP model can be easily extended to the case of three-phase materials (Bendsøe and Sigmund [6]). The difference is that two design variables x_{i1} and x_{i2} are used for element i

$$\begin{aligned}&E\left(\mathbf{x}_i\right) = x_{i2}^r\left(x_{i1}^r E^{(2)} + \left(1 - x_{i1}^r\right)E^{(1)}\right) + \left(1 - x_{i2}^r\right)E^{(0)} \\ &\mathbf{x}_i = \left\{x_{ij}\right\} \quad \left(i = 1,\ldots,n; \quad j = 1,2\right) \\ &E^{(2)} > E^{(1)} > E^{(0)}\end{aligned} \tag{11}$$

Similarly, one can derive the SIMP model for four- and five-phase materials as given in the Appendix.

Consider now the following case. If the three phases consist of two solid materials $E^{(1)}$, $E^{(2)}$ and one void phase $E^{(0)}$=0, the element is then solid if x_{i2}=1, while it is void if x_{i2}=0. Meanwhile, x_{i1} determines which material phase is attributed to element i. Based on many numerical tests (Sun and Zhang [21]), it is found that the structural topology optimization problem can be reasonably stated as:

$$\begin{aligned}&\text{find:} \quad \left\{x_{i1}, x_{i2}\right\} \quad \left(i = 1,\ldots,n\right) \\ &\text{minimize: } C = \mathbf{F}^{\mathrm{T}}\mathbf{u} = \mathbf{u}^{\mathrm{T}}\mathbf{K}\mathbf{u} \\ &\text{subject to: } \mathbf{F} = \mathbf{K}\mathbf{u} \\ &\sum_{i=1}^{n} V_i x_{i2} \le (vf_1 + vf_2)\cdot\sum_{i=1}^{n} V_i; \ \sum_{i=1}^{n} V_i x_{i1} \le vf_2 \cdot \sum_{i=1}^{n} V_i\end{aligned} \tag{12}$$

In this model, the first inequality is added to limit the total cost of solid materials 1 and 2, while the second one is to limit the cost of material 2. Both constraints are thus linear functions of design variables.

Similarly, based on the SIMP model of three-phase materials, we have

$$\begin{aligned}\frac{\partial \mathbf{K}}{\partial x_{i1}} &= \frac{\partial \mathbf{K}_i}{\partial x_{i1}} = x_{i2}^r\left(r x_{i1}^{r-1}\left(\mathbf{K}^{(2)} - \mathbf{K}^{(1)}\right)\right) \\ \frac{\partial \mathbf{K}}{\partial x_{i2}} &= \frac{\partial \mathbf{K}_i}{\partial x_{i2}} = r x_{i2}^{r-1}\left(\left(x_{i1}^r\mathbf{K}^{(2)} + \left(1 - x_{i1}^r\right)\mathbf{K}^{(1)}\right) - \mathbf{K}^{(0)}\right)\end{aligned} \tag{13}$$

In case of fixed load, the sensitivity of the structural compliance can be easily obtained as

$$\begin{aligned}\frac{\partial C}{\partial x_{i1}} &= -x_{i2}^r p x_{i1}^{r-1}\left(E^{(2)} - E^{(1)}\right)\mathbf{u}_i^{\mathrm{T}}\overline{\mathbf{K}}_i\mathbf{u}_i \\ \frac{\partial C}{\partial x_{i2}} &= -\mathbf{u}_i^{\mathrm{T}}\left(r x_{i2}^{r-1}\left(\left(x_{i1}^r\mathbf{K}^{(2)} + \left(1 - x_{i1}^r\right)\mathbf{K}^{(1)}\right) - \mathbf{K}^{(0)}\right)\right)\mathbf{u}_i \\ &= -r x_{i2}^{r-1}\left(\left(x_{i1}^r E^{(2)} + \left(1 - x_{i1}^r\right)E^{(1)}\right) - E^{(0)}\right)\mathbf{u}_i^{\mathrm{T}}\overline{\mathbf{K}}_i\mathbf{u}_i\end{aligned} \tag{14}$$

Instead, in case of design-dependent load, evaluations of $\partial\mathbf{F}/\partial x_{i1}$ and $\partial\mathbf{F}/\partial x_{i2}$ become difficult and will be discussed in Section 3 and 4.

In the same way, for a number of m+1 phase materials of Young's modulus of $E^{(m)}$, …,$E^{(1)}$, $E^{(0)}$ we will have m number of design variables denoted to be x_{im}, …, x_{i2}, x_{i1} for element i. Note that $E^{(0)}$=0 is set to represent the void element and x_{im} represents the absence(0) or existence (1) of solid material phase.

2.3 Numerical strategy of topology optimization

Historically , several approximation schemes have been developed and applied successfully, such as CONLIN (Convex Linearization Method, derived by Fleury and Braibant [11]) and MMA (Svanberg [22]) family. In this paper, the MDQA (Method of Diagonal Quadratic Approximations, by Zhang and Fleury [25]) is applied to solve the topology optimization problem defined in eq. (3) and (12). As the MDQA is an algorithm based on the non-monotonic, convex and second-order approximation in which the diagonal terms of the Hessian matrix are calculated using the function value at the preceding iteration, it is therefore suitable to deal with the optimization problem of design-dependent load for which the objective function is a non-monotonic function. Besides, the filtering technique proposed by Sigmund [18] is adopted herein to avoid the checkerboard.

3 Modeling of unidirectional pressure load on fixed surface

3.1 Load distribution model

As the amount of pressure load, P_{sw}, is unchanged in the optimization process and often defined by the solid weight that the concerned structure supports, it can be described as

$$p \cdot S = P_{\mathrm{sw}} \tag{15}$$

where p is the pressure value depending upon the applied surface area, S. In finite element analysis, the solid weight pressure is usually treated as a uniform pressure, i.e. p=P_{sw}/S. However, in topology optimization, the pressure

value p will vary because S is modified iteratively. To characterize the effect of such a design-dependent load, an exponential penalization scheme is suggested in order to connect the pressure applied on each element to the involved design variable.

As only the design variable x_{im} is concerned to distinguish its solid/void state of each element, for an element located on the load-applied surface, the pressure exists provided the element is a solid one with x_{im}=1 whatever the material phase is. Thus, the pressure on element i is expressed as

$$p_i = x_{im}^s p \tag{16}$$

where s is the penalization factor. From eq. (15), we have

$$\sum_{\xi=1}^{n_s} p_\xi S_\xi = P_{sw} \tag{17}$$

where n_s is the element number on the load-applied surface and S_ξ is the applied surface area of a single element. Then, the substitution of eq. (16) into eq. (17) yields

$$p = \frac{P_{sw}}{\sum_{\xi=1}^{n_s} x_{\xi m}^s S_\xi} \tag{18}$$

The pressure on element i is then equal to

$$p_i = \frac{x_{im}^s}{\sum_{\xi=1}^{n_s} x_{\xi m}^s S_\xi} P_{sw} \tag{19}$$

Therefore, by means of eq. (19), the pressure will be redistributed on each element after each iteration. As an example, consider a structure of two phase materials (solid-void) shown in Fig. 4. Due to the varying distribution of material density along the loading top surface, an uneven pressure distribution will be applied.

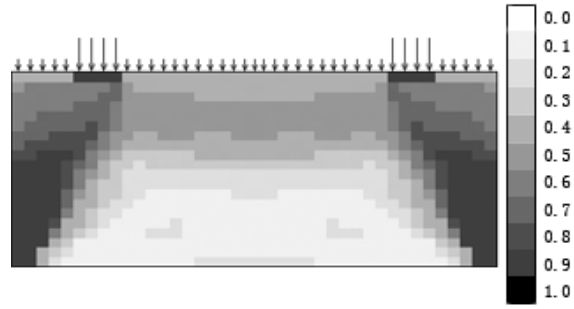

Fig. 4 Pressure load distribution using eq.(19)

3.2 Sensitivity analysis

Because the pressure is only applied on the elements attached to the applied surface, the elements can be divided into two groups for which the force sensitivity term, $\partial \mathbf{F}/\partial x_{ij}$ in eq. (7), is calculated in different ways.

$$\frac{\partial \mathbf{F}}{\partial x_{ij}} = \begin{cases} \sum_{\varsigma=1}^{n_s} \frac{\partial \mathbf{F}_\varsigma}{\partial x_{ij}} & j = m, \text{element } i \in S \\ 0 & \text{others} \end{cases} \tag{20}$$

where $\mathbf{F}_\varsigma$ is the element nodal force vector depending upon p_ς

$$\mathbf{F}_\varsigma = \int_{S_\varsigma} \mathbf{N}_\varsigma^{\mathrm{T}} p_\varsigma ds \tag{21}$$

with $\mathbf{N}_\varsigma$ and S_ς to be the shape function matrix and applied surface of the element.

Based on eq. (19), the partial derivative of p_ς with respect to x_{im} can be derived as

$$\frac{\partial p_\varsigma}{\partial x_{im}} = \begin{cases} \dfrac{\left(s x_{im}^{s-1}\right)\left(\sum_{\xi=1}^{n_s} x_{\xi m}^s S_\xi\right) - \left(x_{im}^s\right)\left(s x_{im}^{s-1} S_i\right)}{\left(\sum_{\xi=1}^{n_s} x_{\xi m}^s S_\xi\right)^2} P_{sw} = \dfrac{s x_{im}^{s-1} \sum_{\xi=1,\xi\neq i}^{n_s} x_{\xi m}^s S_\xi}{\left(\sum_{\xi=1}^{n_s} x_{\xi m}^s S_\xi\right)^2} P_{sw} & \varsigma = i \\ -\dfrac{\left(x_{\varsigma m}^s\right)\left(s x_{im}^{s-1} S_i\right)}{\left(\sum_{\xi=1}^{n_s} x_{\xi m}^s S_\xi\right)^2} P_{sw} = -\dfrac{s x_{im}^{s-1} x_{\varsigma m}^s S_i}{\left(\sum_{\xi=1}^{n_s} x_{\xi m}^s S_\xi\right)^2} P_{sw} & \varsigma \neq i \end{cases} \tag{22}$$

Finally, the sensitivity $\partial C/\partial x_{ij}$ can be obtained.

4 Modeling of unidirectional pressure load on the moving surface

To make things clear, consider a rectangle 2D domain meshed with $n_v \times n_w$ elements as shown in Fig. 5(a). A vector $\{v, w\}$ is used to describe the position of element i in the mesh. Thus, any corresponding parameters associated with element i will be denoted expressed with subscript vw, e.g., x_{vwm} in place of x_{im}.

4.1 Bandwidth load distribution model

Now, the problem is to determine on which elements the pressure load will be applied and how the pressure load will follow the variation of material densities over the mesh. Without loss of generality, consider gray elements of column w along the load direction in Fig. 5(a). They are numbered as 1 to n_w from top to bottom. Herein, a band-

width load distribution model is proposed. For all elements of column w, only the elements that satisfy the following condition will be chosen for load application.

$$\begin{aligned} & x_{\xi wm} > x_{\min} \\ & x_{(\xi+1)wm} > x_{\xi wm} \quad \left(1 \le L_w \le \xi < U_w \le n_{\mathrm{v}}\right) \end{aligned} \tag{23}$$

L_w and U_w denote the numbering of those elements whose x_{vwm} is larger than x_{min} and increases when ξ changes continuously from L_w to U_w along the load direction.

As shown in Fig. 5(a), the bandwidth of loaded elements is marked by dark gray elements for column w. By means of eq. (23), the bandwidth of loaded elements can be identified column by column for the elements of the overall domain. For the material density distribution given in Fig. 5(b), the sub-domain surrounded with black boundary defines the bandwidth of the loaded elements.

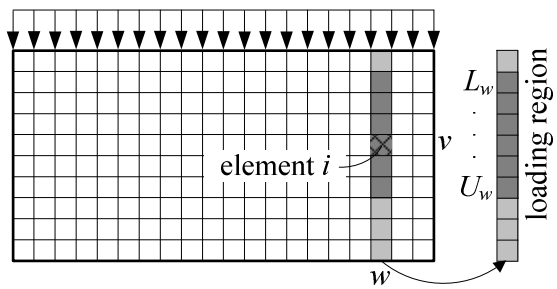

(a) illustration of loaded elements

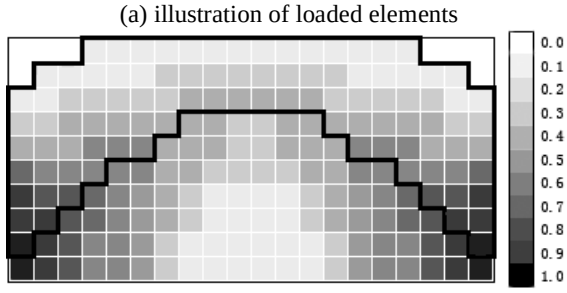

(b) Bandwidth of the loaded elements

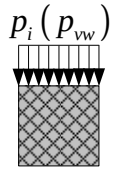

(c) pressure load on one element

Fig. 5 Determination of loaded elements

To determine the distribution of pressure load on the elements in the identified bandwidth, an exponential penalization scheme is introduced.

$$p_{vw} = \begin{cases} x_{vwm}^{s} p_w & L_w \le v \le U_w \\ 0 & v < L_w, v > U_w \end{cases} \tag{24}$$

where s is the penalization factor and the p_w is the segmental pressure for column w. Because the amount of pressure on each column is identical and constant, we have

$$\sum_{\xi=1}^{n_{\mathrm{w}}} p_{\xi w} = p \tag{25}$$

Then, the substitution of eq. (24) into eq. (25) yields

$$p_w = \frac{p}{\sum_{\xi=L_w}^{U_w} x_{\xi wm}^{s}} \tag{26}$$

Accordingly, the pressure on element i corresponds to

$$p_i = p_{vw} = \begin{cases} \dfrac{x_{vwm}^{s}}{\sum_{\xi=L_w}^{U_w} x_{\xi wm}^{s}} p & L_w \le v \le U_w \\ 0 & v < L_w, \quad v > U_w \end{cases} \tag{27}$$

which is applied on the top edge of the element, as shown in Fig. 5(c). Thus, the loads on each element in the bandwidth region are calculated and applied on the corresponding element in each iteration. Fig. 6 shows how the pressure load applied in Fig. 5(a) distributes along with the distribution of density variable. It can be imagined that the load will be only applied on the top side of solid element in each column when a 0-1 pattern of the optimal structure is obtained in case of snow pressure load.

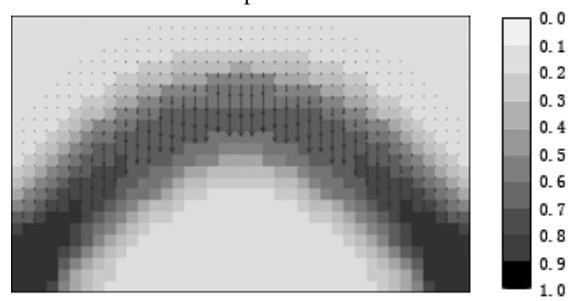

Fig. 6 Distribution of pressure load using Eqs. (23, 27)

4.2 Sensitivity analysis

With the proposed scheme, the load distribution and the bandwidth loaded area will be updated in the FE model after each design iteration. In other words, the design-dependent effect is taken into account only at the stage of finite element analysis.

5 Numerical examples

In this section, 2D models and 3D models are presented, as shown in Fig. 7. The design-dependent pressure is applied in model 2, 3, 5 and 6. Comparatively, the fixed pressure is applied on the non-designable domain of the structure in model 1 and 4. Note that the structure is fixed at the upper corners in model 3, while in other models, the structure is fixed at the lower corners.

In order to compare the results in a coherent way, the normalized objective function $C_{\mathrm{F}}^{\mathrm{r}}$ is used here

$$C_{\mathrm{F}}^{\mathrm{r}} = C / C_{\mathrm{F}} \tag{28}$$

where C is the structural compliance of the optimal structure and C_{F} is that of the initial structure full of material phase m for the problem of m+1 material phases.

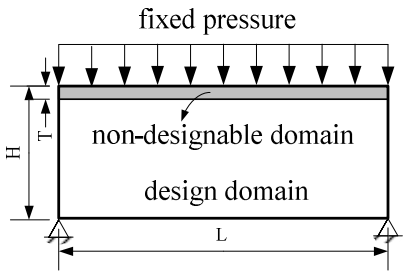

(a) model 1

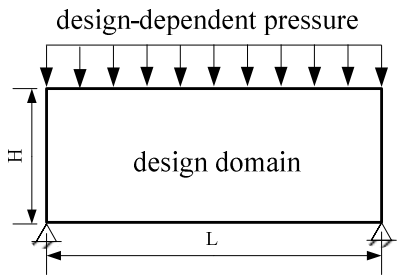

(b) model 2

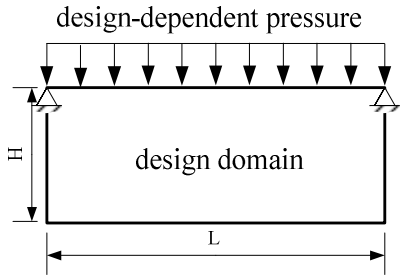

(c) model 3

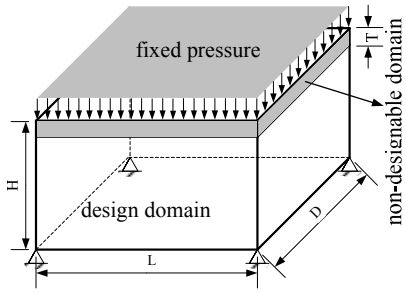

(a) model 4

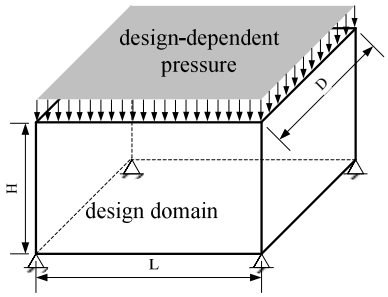

(b) model 5

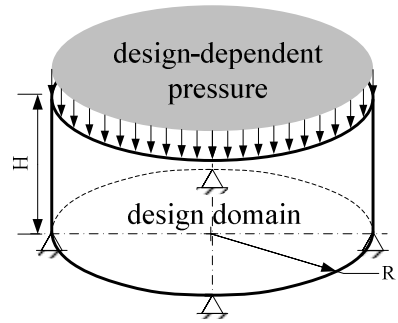

(c) model 6

Fig. 7 Models and boundary conditions

5.1 Unidirectional pressure load on contact surface of fixed shape

2D cases: the optimization of plane examples is firstly presented. Suppose the structure consists of solid and void phase materials and the former is constraint to be 30% volume fraction of the whole structure. For model 2 with L=1 and H=0.4, it is meshed with 120×60 elements. To show the influence of design-dependent effects, the optimal configurations using eq. (7) and eq. (9) for sensitivity analysis are compared in Fig. 8. It can be seen that two inclined columns shown in Fig. 8(a) are joined together by a horizontal member and the pressure loads are concentrated at two extreme ends and transferred to the fixation along the inclined columns. However, if the effect of design-dependent load is ignored in sensitivity analysis, an optimal configuration of reverse "V" shape is obtained and the pressure is applied at the middle part. A comparison of the normalized compliances between two configurations indicates that the configuration given in Fig. 8(a) is much stiffer.

(a) Optimal solution with design-dependent load for model 2 using eq. (7)

$C_F^r = 1.354$

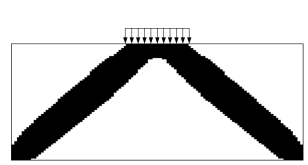

(b) Optimal solution with design-dependent load for model 2 using eq. (9)

$C_F^r = 2.665$

(c) Optimal solution with two-phase solid materials and design-dependent load for model 2 using (eq. (7))

$C_F^r = 1.771$

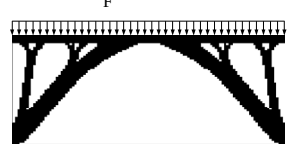

(d) Optimal solution with non-designable domain and fixed load for model 1 using eq. (9)

$C_F^r = 1.624$

Fig. 8 2D optimal configurations with different pressure load models

Besides, the optimal configuration with two solid material phases is presented as well in Fig. 8(c). Herein,

$E^{(2)}$:$E^{(1)}$=3:1 and vf_1=vf_2= 0.15. It is obvious that the stiffer material is distributed along the columns and the middle part of the horizontal member.

In Fig. 8(d), an arch-like structure with small vertical supports is obtained for model 1 under fixed pressure. Here, the volume fraction is set to be 30% of the whole structure for the material constraint and the thickness of the non-designable member consists of four-layer elements.

To reveal the influence of the thickness of the non-designable member, the structural compliance of the optimal solution is plotted versus the thickness in Fig. 9. Following remarks can be made. Firstly, the structural compliance attains the smallest value when four-layer elements are used. Secondly, the structural compliance is always larger than the value obtained by virtue of Eq. (7) that takes into account the design-dependent effect of the pressure load. But it is always smaller than the value obtained by virtue of Eq. (9) that excludes the design-dependent effect of the pressure load in sensitivity analysis.

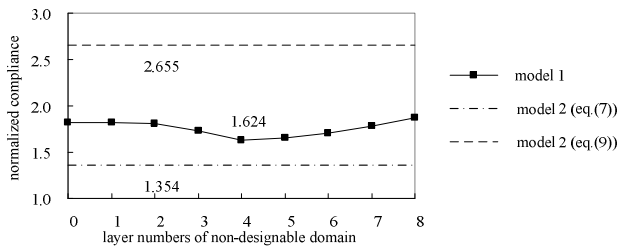

Fig.9 Influence of non-designable member thickness in model 1

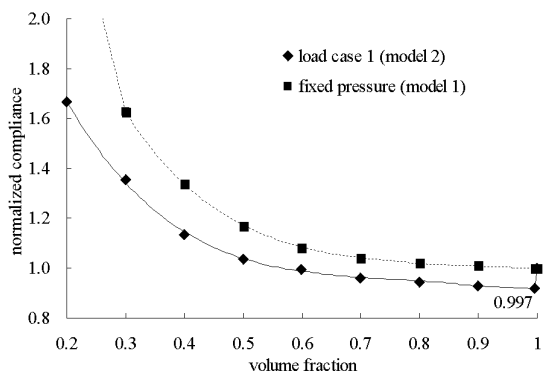

(a) Influence of volume fraction upon normalized compliance

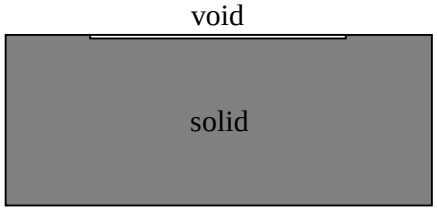

(b) Optimal configuration (model 2, vf_1=0.997)

Fig.10 Optimization results for models 1 and 2

Effects of the volume fraction upon normalized compliance of optimization results are studied in Fig.10(a). For model 1 under fixed pressure, the structural compliance of the optimal design decreases monotonously when the volume fraction increases. This curve agrees well with the concept of conventional topology design, i.e., more material, stiffer the structure. For the structure in load case 1, the curve is found to be non-monotonous. With the increase of the volume fraction, the compliance decreases smoothly and then increases very quickly near vf_1=0.997. It is observed that only the middle part of the top layer is void in the corresponding configuration, as shown in Fig.10(b).

3D cases: models 4-6 shown in Fig. 7 are investigated. Suppose the volume fraction is set to be 15% of the whole structure. Dimensions are L=D=1 and H=0.4 for models 4 and 5, R=1 and H=0.4 for model 6. Note that the top layer elements are assumed to be non-designable for fixed pressure in model 4.

The optimal designs of three models are shown in Fig. 11. For model 4, the optimal configuration given in Fig. 11(a) is similar to that found by Yang et al. (2005). For models 5 and 6, four columns are generated on the fixed points and connected by straight members. The comparison shows that the solution without non-designable domain has smaller compliance value than that in Fig. 11(a).

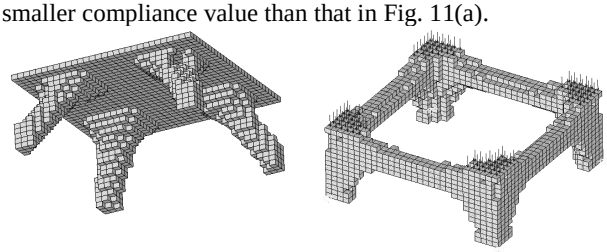

(a) optimal structure of model 4 $C_F^r = 1.487$

(b) optimal structure of model 5 $C_F^r = 1.056$

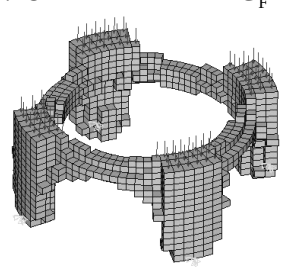

(c) optimal structure of model 6 $C_F^r = 1.167$

Fig. 11 3D optimal configurations

5.2 Unidirectional pressure load on the moving surface

Model 2 is investigated firstly. Dimensions are L=1 and H=0.5. The structure is meshed with 40×20 elements. The optimal design is shown in Fig. 12(b) while the optimal design from the literature is shown in Fig. 12(a) for comparison. The former is found to be more interesting with a smaller value of structural compliance.

In Fig. 12(c), the optimal solution associated with two-solid phase materials is illustrated. Besides, effects of the volume fraction upon the normalized compliance are plotted in Fig.13. Obviously, the compliance of optimal structure decreases very slowly when the volume fraction is

larger than 0.6. Some representative optimal configurations are presented in Fig.13 as well.

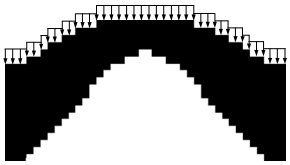

(a) two material phases (Du and Olhoff [9])
vf_1=0.5, $C_F^r = 1.071$

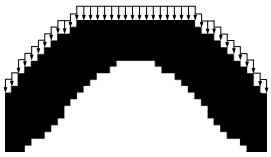

(b) two material phases
vf_1=0.5, $C_F^r = 1.051$

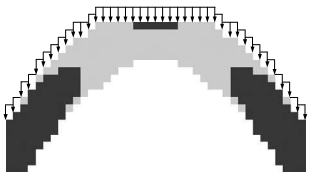

(c) three material phases
vf_1= vf_2=0.2, $E^{(2)}$:$E^{(1)}$=3:1
$C_F^r = 1.771$

Fig. 12 2D optimal configurations of model 2 under pressure load of case 2

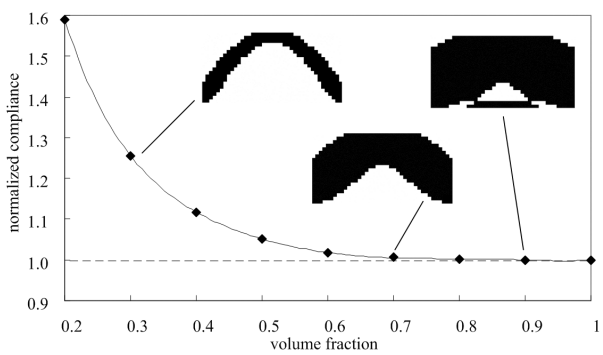

Fig. 13 Normalized compliance versus volume fraction for optimization results of model 2 under pressure load of case 2

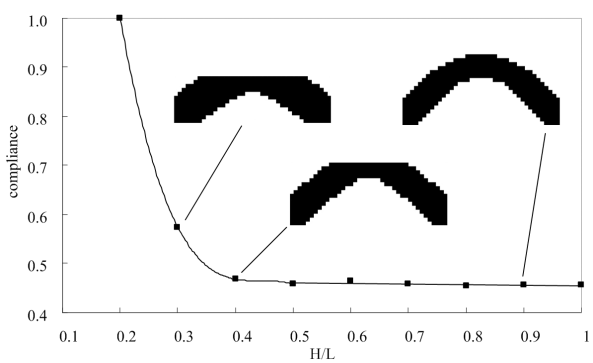

Fig.14 Influence of H/L upon the optimization results

Now, it is interesting to investigate the influence of structural dimension upon the optimization results. Here, dimension H is assumed to be changeable while L=1 is retained and the volume of solid material is kept to be 0.2 irrespective of H. Optimal solutions for different values of H are presented in Fig. 14. One can see that the structural compliance decreases with the increase of H. And that the optimal configurations are almost kept to be unchanged when $H \geq 0.5$, i.e., the optimization result cannot be improved any more.

Furthermore, the proposed design procedure is applied for model 3 that is fixed at the upper corners. The design domain has a dimension of L=1 and H=0.5 and is meshed into 40×20 elements. Under the moving pressure load, the optimization results of one and two solid material phases are shown in Fig.15, respectively. Both configurations are found to be similar and no elements of intermediate density values exist.

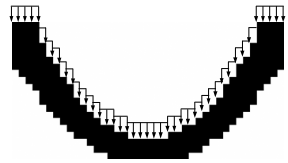

(a) one solid material phase
vf_1=0.3, $C_F^r = 1.253$

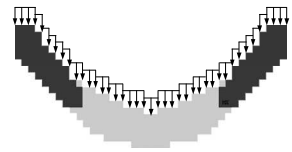

(b) two solid material phases
vf_1= vf_2= 0.15,
$E^{(2)}$:$E^{(1)}$=3:1, $C_F^r = 1.788$

Fig. 15 2D optimal configurations of model 3 under pressure load of case 2

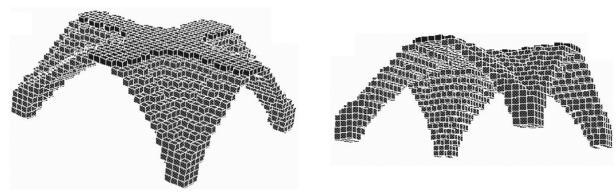

(a) optimal structure of model 5 (Yang et al. [24])
$C_F^r = 1.379$

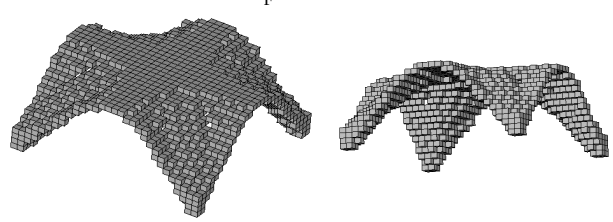

(b) optimal structure of model 5
$C_F^r = 1.373$

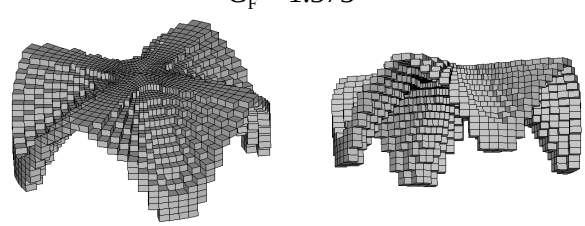

(c) optimal structure of model 6
(d) $C_F^r = 1.344$

Fig. 16 3D optimal configurations under pressure load of case 2

3D cases: The optimal designs of 3D problems under load case 2 are shown in Fig. 16. The same dimensions as those in Fig. 11 are adopted and vf_1=0.1. For model 5, the optimal configuration given in Fig. 16(b) is very similar to that obtained by Yang et al. [24] and shown in Fig. 16(a). Both optimization results of model 5 and 6 resemble the

gothic vaulting. Obviously, four arches join the adjacent supports. Moreover, there are two arch vaults over the diagonal supports and a cross appears at the top of the structure.

Conclusions

This work is focused on topology optimization of structures consisting of multiphase materials under unidirectional pressure load. Unlike traditional design problems, the unidirectional pressure load considered here is design-dependent. This means that the pressure load varies in magnitude and location with respect to the material distribution. Exponential models of closed-form are proposed to describe the relationship between the pressure load and the material density variables. Correspondingly, sensitivity analysis is developed to take into account the design-dependent effect of the load variation during the design iteration. As the structural compliance is no longer monotonic function of design variables, the MDQA optimization algorithm is adopted to solve the considered numerical examples. The investigation of obtained results shows that the developed force model and the design procedure are reliable to produce satisfactory design solutions.

Acknowledgements

This study is supported by the 973 Program (2006CB601205) and National Natural Science Foundation of China (50775184).

References

1. G. Allaire, F. Jouve, A-M. Toader, *Structural optimization using sensitivity analysis and a level-set method*, J Comput Phys, **194**, 363-393 (2004).
2. R. Ansola, J. Canales, A.J. Tárrago, *An efficient sensitivity computation strategy for the evolutionary structural optimization (ESO) of continuum structures subjected to self-weight loads*, Finite Elements in Analysis and Design, **42**, 1220-123 (2006).
3. M.P. Bendsøe, *Optimal shape design as a material distribution problem*. Struct Optim, **10**, 193-202 (1989).
4. M.P. Bendsøe, *Optimization of Structural Topology, Shape, and Material*. (Springer, London UK. 1995).
5. M.P. Bendsøe, N. Kikuchi, *Generating optimal topologies in structural design using homogenization.* Comput Methods Appl Mech Eng, **71**, 197-224 (1988).
6. M.P. Bendsøe, O. Sigmund, *Material interpolation in topology optimization*. Arch Appl Methods, **69**, 635-654 (1999).
7. M. Bruyneel, P. Duysinx, *Note on topology optimization of continuum structures including self-weight*. Struct Multidisc Optim, **29**, 245-256 (2005).
8. B.C. Chen, N. Kikuchi, *Topology optimisation with design dependent loads*. Finite Elem Anal Des, **39**, 57-70 (2001).
9. J. Du, N. Olhoff, *Topological optimization of continuum structures with design-dependent surface loading - Part I: new computational approach for 2D problems*. Struct. Multidisc. Optim, **27**, 166-177 (2003).
10. J. Du, N. Olhoff, *Topological optimization of continuum structures with design-dependent surface loading - Part II: algorithm and examples for 3D problems*. Struct. Multidisc. Optim, **27**, 151-165 (2003).
11. C. Fleury, V. Braibant, *Structural optimization: A new dual method using mixed variables*. Int J Numer Methods Eng, **23**, 409– 428 (1986).
12. M.B. Fuchs, E. Moses, *Optimal structural topologies with transmissible loads*. Struct Multidisc Optim, **19**, 263-73 (2000).
13. M.B. Fuchs, N.N.Y. Shemesh, *Density-based topological design of structures subjected to water pressure using a parametric loading surface*. Struct Multidisc Optim, **28**, 11-19 (2004).
14. T. Gao, W.H. Zhang, J.H. Zhu, Y.J Xu, D.H. Bassir, *Topology Optimization of Heat Conduction Problem Involving Design dependent Heat Load Effect*. Finite Elements in Analysis and Design, **44**, 805-813 (2008).
15. V.B. Hammer, N. Olhoff, *Topology optimisation of continuum structures subjected to pressure loading*. Struct Multidisc Optim, **19**, 85-92 (2000).
16. Z. Liu, J.G. Korvink, R. Huang, *Structure topology optimization: fully coupled level set method via FEMLAB*, Struct Multidisc Optim, **29**, 407-417 (2005).
17. G.I.N. Rozvany, W. Prager, *A new class of structural optimisation problems: optimal archgrids*. Comput Methods Appl Mech Eng, **19**, 49-58 (1979).
18. O. Sigmund, *A 99 line topology optimization code written in Matlab*. Struct Multidisc Optim, **21**, 120-127 (2001).
19. O. Sigmund, P.M. Clausen, *Topology optimization using a mixed formulation: An alternative way to solve pressure load problems*. Comput Methods Appl Mech Engrg, **196**, 1874-1889 (2007).
20. M. Stolpe, K. Svanberg, *An alternative interpolation scheme for minimum compliance topology optimization*. Struct Multidisc Optim, **22**, 116-124 (2001).
21. S.P. Sun, W.H. Zhang, *Multiple objective topology optimal design of multiphase microstructures*. Chinese Journal of Theoretical and Applied Mechanics, **38**, 633-638 (2006). (in Chinese)
22. K. Svanberg, *The method of moving asymptotes – a new method for structural optimization*. Int J Numer Methods Eng, **24**, 359-373 (1987).
23. S. Turteltaub, P. Washabaugh, *Optimal distribution of material properties for an elastic continuum with structure-dependent body force*. Int J Solids Struct, **36**, 4587-4608 (1999).
24. X.Y. Yang, Y.M. Xie, G.P. Steven, *Evolutionary methods for topology optimization of continuous structures with design dependent loads*. Computers and Structures, **83**, 956-963 (2005).
25. W.H. Zhang, C. Fleury, *A modification of convex approximation methods for structural optimization*. Computers & Structures, **64**, 89-95 (1997).